DEUTSCHES ELEKTRONEN-SYNCHROTRON
Ein Forschungszentrum der Helmholtz-Gemeinschaft

DESY 20-032
arXiv:2003.01014
March 2020

Dipole Subtraction vs. Phase Space Slicing in NLO NRQCD Heavy-Quarkonium Production Calculations

M. Butenschoen, B. A. Kniehl

II. Institut für Theoretische Physik, Universität Hamburg

ISSN 0418-9833

NOTKESTRASSE 85 - 22607 HAMBURG

To be sure that your reports and preprints are promptly included in the HEP literature database
send them to (if possible by air mail):

DESY Zentralbibliothek Notkestraße 85 22607 Hamburg Germany	DESY Bibliothek Platanenallee 6 15738 Zeuthen Germany

DESY 20–032
February 2020

ISSN 0418-9833

Dipole Subtraction vs. Phase Space Slicing in NLO NRQCD Heavy-Quarkonium Production Calculations

Mathias Butenschoen, Bernd A. Kniehl
II. Institut für Theoretische Physik, Universität Hamburg,
Luruper Chaussee 149, 22761 Hamburg, Germany

March 3, 2020

Abstract

We compare two approaches to evaluate cross sections of heavy-quarkonium production at next-to-leading order in nonrelativistic QCD involving S- and P-wave Fock states: the customary approach based on phase space slicing and the approach based on dipole subtraction recently elaborated by us. We find reasonable agreement between the numerical results of the two implementations, but the dipole subtraction implementation outperforms the phase space slicing one both with regard to accuracy and speed.

PACS numbers: 12.38.Bx, 12.39.St, 13.85.Ni, 14.40.Pq

1 Introduction

The conjectured factorization theorem [1] of nonrelativistic QCD (NRQCD) [2] is the most frequently used framework for calculations of inclusive heavy-quarkonium production. It is based on a factorization into perturbative short-distance cross sections for heavy-quark-antiquark pairs in certain Fock states n, and nonperturbative long-distance matrix elements (LDMEs). The numerical values of the latter are extracted from fits to experimental data, and are predicted to scale with certain powers of the relative heavy-quark-antiquark velocity v [3]. For the phenomenologically important quarkonia, the leading and next-to-leading contributions in the v expansion involve S- and P-wave bound states. Many calculations of these contributions have been performed at next-to-leading order (NLO) in the strong-coupling constant α_s. These works were almost exclusively done using the two-cutoff phase space slicing scheme as described in Ref. [4]. To our knowledge, the only exception is the work of Ref. [5], where color-singlet S-wave-state production was treated in the massless Catani-Seymour dipole subtraction scheme [6]. In Ref. [7], we have formulated a subtraction scheme covering S- and P-wave color-singlet and color-octet states for the important example of hadroproduction. It is based on Ref. [6] and its extension to massive quarks by Phaf and Weinzierl [8]. In particular, it takes into account the bound-state structure of the projected amplitudes and introduces new kinds of subtraction terms for the case of P-wave-state production.

This paper describes a numerical comparison of our implementations of two-cutoff phase space slicing and dipole subtraction for inclusive quarkonium hadroproduction. In Section 2, we briefly review the singularity structure of the encountered real-correction squared amplitudes and their cancellation by other contributions. We summarize phase space slicing in Section 3 and dipole subtraction in Section 4, providing many previously unpublished technical details. In Section 5, we then numerically compare the two implementations, before summarizing our results in Section 6.

2 Singular cross section contributions

The factorization theorems of QCD and NRQCD imply that the inclusive cross section to produce a heavy-quarkonium state H is given by

$$d\sigma(AB \to H + X) = \sum_{a,b,X} \sum_{n} \int dx_a dx_b \, f_{a/A}(x_a) f_{b/B}(x_b) \langle \mathcal{O}^H[n] \rangle d\hat{\sigma}(ab \to Q\overline{Q}[n] + X), \tag{1}$$

with the partonic cross sections

$$\begin{aligned} d\hat{\sigma}(ab \to Q\overline{Q}[n] + X) = {} & \frac{1}{N_{\mathrm{col}}(n) N_{\mathrm{pol}}(n)} \frac{1}{2(p_1 + p_2)^2} \, d\mathrm{PS} \\ & \times \frac{F_{\mathrm{sym}}(X)}{n_{\mathrm{col}}(a) n_{\mathrm{pol}}(a) n_{\mathrm{col}}(b) n_{\mathrm{pol}}(b)} \| |ab \to Q\overline{Q}[n] + X\rangle \|^2. \end{aligned} \tag{2}$$

Here, $f_{a/A}(x_a)$ is the parton distribution function (PDF) describing the probability to find parton a with longitudinal momentum fraction x_a inside hadron A. $\langle \mathcal{O}^H[n] \rangle$ is the LDME of NRQCD associated with the intermediate Fock state n, which has N_{col} color and N_{pol} polarization degrees of freedom. p_1 and p_2 are the four-momenta of partons a and b, n_{col} and n_{pol} their color and spin averaging factors. dPS is the phase space and F_{sym} the symmetry factor associated with the outgoing particles. $|ab \to Q\overline{Q}[n] + X\rangle$ denotes the matrix element of the partonic subprocess $ab \to Q\overline{Q}[n] + X$, which is calculated by applying spin and color projectors to the usual QCD amplitudes as described in Ref. [7]. A summation of spin and color degrees of freedom of the $Q\overline{Q}$ pair and all incoming and outgoing partons is always implicitly understood in the squared amplitudes, but no averaging. At this point, we deviate from the definition of the bra and ket symbols used in Refs. [6,8]. We denote the momentum of the $Q\overline{Q}$ pair as p_0 and set $p_0^2 = 4m_Q^2$, with m_Q being the heavy-quark mass. Our real-correction partonic amplitudes have two further light QCD partons, to which we assign momenta p_3 and p_4.

In the limit where an outgoing gluon with momentum p_j gets soft, the squared production amplitude becomes, for the Fock states considered in our analysis,

$$
\begin{aligned}
&\| |{}^1S_0^{[1/8]}, p_j \text{ soft}\rangle \|^2 = S_1({}^1S_0^{[1/8]}; p_j), \\
&\| |{}^3S_1^{[1/8]}, p_j \text{ soft}\rangle \|^2 = S_1({}^3S_1^{[1/8]}; p_j), \\
&\| |{}^1P_1^{[1/8]}, p_j \text{ soft}\rangle \|^2 = S_1({}^1P_1^{[1/8]}; p_j) + S_2({}^1P_1^{[1/8]}, {}^1S_0^{[1/8]}; p_j) + S_3({}^1S_0^{[1/8]}; p_j), \\
&\| |{}^3P_J^{[1/8]}, p_j \text{ soft}\rangle \|^2 = S_1({}^3P_J^{[1/8]}; p_j) + S_2({}^3P_J^{[1/8]}, {}^3S_1^{[1/8]}; p_j) + S_3({}^3S_1^{[1/8]}; p_j),
\end{aligned} \tag{3}
$$

with

$$
\begin{aligned}
S_1(n; p_j) = g_s^2 \sum_{\substack{i,k=1 \\ i,k\neq j}}^{4} &\left(-\frac{p_i \cdot p_k}{p_i \cdot p_j \; p_k \cdot p_j} + \frac{p_0 \cdot p_i}{p_0 \cdot p_j \; p_i \cdot p_j} + \frac{p_0 \cdot p_k}{p_0 \cdot p_j \; p_k \cdot p_j} - \frac{p_0^2}{(p_0 \cdot p_j)^2} \right) \\
&\times \langle n, \text{Born} | \mathbf{T}_i \mathbf{T}_k | n, \text{Born} \rangle
\end{aligned} \tag{4}
$$

$$
\begin{aligned}
S_2(n, m; p_j) = 4g_s^2 \sum_{\substack{i=1 \\ i\neq j}}^{4} &\left(\frac{-p_i^\beta}{p_i \cdot p_j \; p_0 \cdot p_j} + \frac{p_0 \cdot p_i \; p_j^\beta}{p_i \cdot p_j (p_0 \cdot p_j)^2} - \frac{p_0^2 p_j^\beta}{(p_0 \cdot p_j)^3} \right) \\
&\times \epsilon_\beta(m_l) \langle n, \text{Born} | \mathbf{T}_i (\mathbf{T}_Q - \mathbf{T}_{\overline{Q}}) | m, \text{Born} \rangle
\end{aligned} \tag{5}
$$

$$
\begin{aligned}
S_3(m; p_j) = 4g_s^2 &\left(-\frac{g^{\alpha\beta}}{(p_0 \cdot p_j)^2} - \frac{p_0^2 p_j^\alpha p_j^\beta}{(p_0 \cdot p_j)^4} \right) \\
&\times \epsilon_\alpha^*(m_l) \epsilon_\beta(m_l) \langle m, \text{Born} | (\mathbf{T}_Q - \mathbf{T}_{\overline{Q}}) (\mathbf{T}_Q - \mathbf{T}_{\overline{Q}}) | m, \text{Born} \rangle,
\end{aligned} \tag{6}
$$

where $|m, \text{Born}\rangle$ is the Born amplitude of $Q\overline{Q}[m]$ production without the soft gluon. $\mathbf{T}_i$ acts on $|m, \text{Born}\rangle$ by inserting at the corresponding place T_c if parton i is an outgoing quark or incoming antiquark, $-T_c$ if parton i is an incoming antiquark or outgoing quark, and if_{abc} if parton i is a gluon, where c, a, and b are the color indices of the soft, splitting, and other outgoing gluons, respectively. $\mathbf{T}_Q$ inserts T_c at the place of the outgoing heavy

quark Q, $\mathbf{T}_{\overline{Q}}$ inserts $-T_c$ at the place of the outgoing heavy antiquark $\overline{Q}$, with c being the color index of Q or $\overline{Q}$.

In the limit where an outgoing light parton with momentum p_j becomes collinear to an incoming light parton with momentum p_i, its main contribution stems from Feynman diagrams where parton i splits into j and a parton with momentum $p_{(ij)} = p_i - p_j$ taking away the fraction x of the incoming parton's longitudinal momentum. The squared matrix element in that limit is given by

$$\begin{aligned} \| |p_j \text{ ini. coll. } p_i\rangle \|^2 = \frac{n_{\text{col}}(i)}{n_{\text{col}}((ij))n_{\text{pol}}((ij))} \frac{g_s^2}{x(p_i \cdot p_j)} \langle \text{Born}|\hat{P}_{i,(ij)}(x, p_\perp)|\text{Born}\rangle \\ \times \begin{cases} \delta_{ss'} & \text{if } i \text{ is a quark or antiquark} \\ \epsilon^*_\mu(p_i)\epsilon_\nu(p_i) & \text{if } i \text{ is a gluon} \end{cases}, \end{aligned} \tag{7}$$

where $\hat{P}_{i,(ij)}(x)$ are the spin-dependent Altarelli-Parisi splitting functions as given in Ref. [7]. The squared amplitude in the limit where the outgoing partons 3 and 4 are collinear is given by those Feynman diagrams where a final-state parton with momentum $p_{(34)} = p_3 + p_4$ splits into the outgoing partons 3 and 4, and reads

$$\| |p_3 \text{ final coll. } p_4\rangle \|^2 = \frac{g_s^2}{p_3 \cdot p_4} \langle \text{Born}|\hat{P}_{(34),3}(z, p_\perp)|\text{Born}\rangle. \tag{8}$$

The phase space integrations in $D = 4 - 2\epsilon$ dimensions yield $\frac{1}{\epsilon}$ and $\frac{1}{\epsilon^2}$ poles, which are canceled by similar poles in the virtual corrections, by the *mass factorization counterterms*, and by the *operator renormalization counterterms*: A part of the initial-state collinear singularities is absorbed into the PDFs according to the $\overline{\text{MS}}$ prescription, thereby leading to mass factorization counterterms,

$$\begin{aligned} d\hat{\sigma}_{\text{MFC}}(a + b \to Q\overline{Q}[n] + X) = \Bigg[\sum_{(ij)} \int dx P^+_{a,(ij)}(x) d\hat{\sigma}_{\text{Born}}((ij) + b \to Q\overline{Q}[n] + X) \\ + \sum_{(ij)} \int dx P^+_{b,(ij)}(x) d\hat{\sigma}_{\text{Born}}(a + (ij) \to Q\overline{Q}[n] + X) \Bigg] \frac{g_s^2}{8\pi^2} \left(\frac{4\pi\mu_r^2}{\mu_f^2} e^{-\gamma_E} \right)^\epsilon \frac{1}{\epsilon}, \end{aligned} \tag{9}$$

where μ_r is the renormalization scale, μ_f is the QCD factorization scale, and $P^+_{a,(ij)}(x)$ are the regularized Altarelli-Parisi splitting functions as listed in Ref. [7]. The singularites of the S_3 part of the soft singularities are canceled by NLO corrections to LDMEs, where ultraviolet singularities are removed by $\overline{\text{MS}}$ renormalization. These *operator renormalization* contributions are, for the Fock states relevant to our analysis, given by

$$\begin{aligned} d\sigma_{{}^3S_1^{[1]} + {}^3S_1^{[8]} \text{ op.ren.}} = \sum_{\substack{a,b,X \\ 2\to 2}} \sum_{c=1,8} \sum_J \int dx_a dx_b \, f_{a/A}(x_a) f_{b/B}(x_b) \frac{\langle \mathcal{O}^H[{}^3P_J^{[c]}] \rangle}{N_{\text{col}}({}^3P_J^{[c]}) N_{\text{pol}}({}^3P_J^{[c]})} \\ \times \frac{1}{2(p_1 + p_2)^2} \, d\text{PS}_2 \frac{F_{\text{sym}}(X)}{n_{\text{col}}(a) n_{\text{pol}}(a) n_{\text{col}}(b) n_{\text{pol}}(b)} \| |{}^3P_J^{[c]}, \text{ op.ren.}\rangle \|^2, \end{aligned} \tag{10}$$

with

$$\||^3P_J^{[c]}, \text{op.ren.}\rangle\|^2 = \frac{g_s^2}{12\pi^2 m_Q^2}\left(\frac{4\pi\mu_r^2}{\mu_\Lambda^2}e^{-\gamma_E}\right)^\epsilon g^{\alpha\beta}\left(-\frac{1}{\epsilon}\right) \times \epsilon_\alpha^*(m_l)\epsilon_\beta(m_l)\langle {}^3S_1^{[c]}, \text{Born}|(\mathbf{T}_Q - \mathbf{T}_{\overline{Q}})(\mathbf{T}_Q - \mathbf{T}_{\overline{Q}})|{}^3S_1^{[c]}, \text{Born}\rangle, \quad (11)$$

and

$$d\sigma_{{}^1S_0^{[1]}+{}^1S_0^{[8]}\,\text{op.ren.}} = \sum_{\substack{a,b,X\\2\to 2}}\sum_{c=1,8}\int dx_a dx_b\, f_{a/A}(x_a) f_{b/B}(x_b)\frac{\langle \mathcal{O}^H[{}^1P_1^{[c]}]\rangle}{N_{\text{col}}({}^1P_1^{[c]})N_{\text{pol}}({}^1P_1^{[c]})} \times \frac{1}{2(p_1+p_2)^2}\,d\text{PS}_2\frac{F_{\text{sym}}(X)}{n_{\text{col}}(a)n_{\text{pol}}(a)n_{\text{col}}(b)n_{\text{pol}}(b)}\||^1P_1^{[c]}, \text{ op.ren.}\rangle\|^2, \quad (12)$$

with

$$\||^1P_1^{[c]}, \text{op.ren.}\rangle\|^2 = \frac{g_s^2}{12\pi^2 m_Q^2}\left(\frac{4\pi\mu_r^2}{\mu_\Lambda^2}e^{-\gamma_E}\right)^\epsilon g^{\alpha\beta}\left(-\frac{1}{\epsilon}\right) \times \epsilon_\alpha^*(m_l)\epsilon_\beta(m_l)\langle {}^1S_0^{[c]}, \text{Born}|(\mathbf{T}_Q - \mathbf{T}_{\overline{Q}})(\mathbf{T}_Q - \mathbf{T}_{\overline{Q}})|{}^1S_0^{[c]}, \text{Born}\rangle, \quad (13)$$

where μ_Λ is the NRQCD factorization scale.

3 Phase space slicing implementation

Our implementation of phase space slicing follows the lines of Ref. [4]. Here, the real-correction phase space is split into three regions by introducing two cut-off parameters, δ_s and δ_c: The soft region, where p_3 or p_4 is soft, the hard-collinear region, where p_3 and p_4 are hard and p_3 or p_4 is collinear to another massless parton, and the hard-noncollinear region. The condition of p_j being soft is defined by $\delta_s > 2E_j/\sqrt{s}$ and the condition of p_i being collinear to p_j by $\delta_c > |2p_i\cdot p_j|/\sqrt{s}$ with $s = (p_1+p_2)^2$. Since the hard-noncollinear region is free of singularities, the phase space integration is done there numerically, while, in the other two regions, the phase space integrations are done analytically in $D = 4-2\epsilon$ dimensions. This is possible because not only the squared matrix elements factorize as described above, but also the phase space elements factorize, schematically as $d\text{PS}_3 = d\text{PS}_2 d\text{PS}_{p_j}$, where p_j is soft, and $d\text{PS}_3 = d\text{PS}_2 d\text{PS}_{p_i\|p_j}$, where p_i is collinear to p_j. Here,

$$d\text{PS}_{p_j} = \frac{d^{D-1}p_j}{2(2\pi)^{D-1}E_j}, \qquad d\text{PS}_{p_i\|p_j} = \begin{cases} \frac{d^{D-1}p_j}{2(2\pi)^{D-1}E_j} & \text{if } i=1,2 \text{ and } j=3,4 \\ \frac{d^{D-1}p_j}{2(2\pi)^{D-1}}\frac{E_{(ij)}}{E_iE_j} & \text{if } i \text{ and } j = 3,4 \end{cases}. \quad (14)$$

The dependencies of all contributions on δ_s and δ_c cancel in the sum.

3.1 Hard-collinear part

Integrating Eq. (7) analytically over the hard-collinear phase space part and adding the corresponding contribution of the mass factorization counterterm in Eq. (9), we obtain in the limit $\delta_s \to 0$

$$\left[\int_{p_i \| p_j} d\mathrm{PS}_{p_i\|p_j} \| |p_i \text{ ini. coll. } p_j\rangle\|^2\right]_{+\mathrm{MFC}} = \int_{x_{\min}}^{1-\delta_s\delta_{j,g}} dx \| |\mathrm{Born}\rangle\|^2 \Bigg[\delta(1-x) F_{\mathrm{in},i\to(ij),j} + \frac{g_s^2}{8\pi^2}\left(P_{i,(ij)}(x)\ln\frac{(1-x)\delta_c s}{\mu_f^2} - P'_{i,(ij)}(x)\right)\Bigg], \tag{15}$$

where the Born amplitude $|\mathrm{Born}\rangle$ is defined with an incoming momentum $p_{(ij)} = x p_i$ instead of p_i. $\delta_{j,g}$ is 1 if particle j is a gluon, otherwise 0. $F_{\mathrm{in},i\to(ij),j}$ are given by

$$\begin{aligned} F_{\mathrm{in},g\to gg} &= \frac{g_s^2}{8\pi^2} C_\epsilon \left(\frac{1}{\epsilon} + \ln\frac{m_Q^2}{\mu_f^2}\right)\left(2C_A \ln\delta_s + \frac{11}{6}C_A - \frac{n_f}{3}\right), \\ F_{\mathrm{in},q\to qg} &= \frac{g_s^2}{8\pi^2} C_\epsilon \left(\frac{1}{\epsilon} + \ln\frac{m_Q^2}{\mu_f^2}\right)\left(2\ln\delta_s + \frac{3}{2}\right), \end{aligned} \tag{16}$$

with $C_A = 3$, $C_F = 4/3$, and $C_\epsilon = (4\pi\mu_r^2 e^{-\gamma_E}/m_Q^2)^\epsilon$. Furthermore, $P_{i,(ij)}$ and $P'_{i,(ij)}$ are the $\mathcal{O}(\epsilon^0)$ and $\mathcal{O}(\epsilon)$ parts of the spin-averaged splitting functions, namely

$$\begin{aligned} P_{qq}(x) &= C_F \frac{1+x^2}{1-x}, \\ P'_{qq}(x) &= -C_F(1-x), \\ P_{qg}(x) &= C_F \frac{1+(1-x)^2}{x}, \\ P'_{qg}(x) &= -C_F x, \\ P_{gg}(x) &= 2C_A\left(\frac{x}{1-x} + \frac{1-x}{x} + x(1-x)\right), \\ P'_{gg}(x) &= 0, \\ P_{gq}(x) &= \frac{1}{2}\left(x^2 + (1-x)^2\right), \\ P'_{gq}(x) &= -x(1-x). \end{aligned} \tag{17}$$

Integrating Eq. (8) analytically over the hard-collinear phase space part, we obtain in the limit $\delta_s \to 0$

$$\int_{p_3\|p_4} d\mathrm{PS}_{p_3\|p_4} \| |p_3 \text{ fin. coll. } p_4\rangle\|^2 = \| |\mathrm{Born}\rangle\|^2 F_{\mathrm{fi},(34)\to 3,4}, \tag{18}$$

with

$$F_{\mathrm{fi},g\to gg} = \frac{g_s^2 C_A}{8\pi^2} C_\epsilon \left[\left(\frac{1}{\epsilon} - \ln\frac{\delta_c s}{m_Q^2}\right)\left(\frac{11}{6} + 2\ln\frac{s\delta_s}{s-4m_Q^2}\right) - \ln^2\frac{\delta_s s}{s-4m_Q^2} + \frac{67}{18} - \frac{\pi^2}{3}\right],$$

$$F_{\mathrm{fi},g\to q\overline{q}} = \frac{g_s^2}{8\pi^2}\frac{n_f}{3} C_\epsilon \left[-\frac{1}{\epsilon} + \ln\frac{\delta_c s}{m_Q^2} - \frac{5}{3}\right],$$

$$F_{\mathrm{fi},q\to qg} = \frac{g_s^2 C_F}{8\pi^2} C_\epsilon \left[\left(\frac{1}{\epsilon} - \ln\frac{\delta_c s}{m_Q^2}\right)\left(\frac{3}{2} + 2\ln\frac{\delta_s s}{s-4m_Q^2}\right) - \ln^2\frac{\delta_s s}{s-4m_Q^2} + \frac{7}{2} - \frac{\pi^2}{3}\right]. \quad (19)$$

3.2 Soft part: S_1 terms

The integral of the S_1 terms in Eq. (4) over the soft phase space region can be written as

$$\int_{p_j \text{ soft}} d\mathrm{PS}_{p_j} S_1(n, p_j) = g_s^2 \left(-C_{00} I_{00} - \sum_{\substack{i,k=0 \\ \{i,j,k\}\,\text{distinct}}}^{4} 2 C_{ik} I_{ik}\right), \quad (20)$$

with

$$C_{ik} = \langle \mathrm{Born}|\mathbf{T}_i \mathbf{T}_k|\mathrm{Born}\rangle, \qquad I_{ik} = \int_{p_j \text{ soft}} d\mathrm{PS}_{p_j} \frac{p_i \cdot p_k}{p_i \cdot p_j \; p_k \cdot p_j}, \quad (21)$$

where we define $\mathbf{T}_0 = \mathbf{T}_Q + \mathbf{T}_{\overline{Q}}$ and use $\mathbf{T}_i = -\sum_{k\neq i,j}^{4} \mathbf{T}_k$, with p_j being the soft momentum. Evaluating the integrals I_{ik} following Ref. [4], we obtain

$$\begin{aligned}
I_{0,0} &= \frac{1}{8\pi^2} C_\epsilon \left[-\frac{1}{\epsilon} - \frac{s+4m_Q^2}{s-4m_Q^2}\ln\frac{s}{4m_Q^2} + \ln\frac{\delta_s^2 s}{m_Q^2}\right], \\
I_{0,k=1\,\text{or}\,2} &= \frac{1}{16\pi^2} C_\epsilon \left[\frac{1}{\epsilon^2} - \frac{1}{\epsilon}\ln\frac{\psi_k^2\delta_s^2}{4m_Q^4} + \ln^2\frac{-\psi_k^2}{4m_Q^2} - \frac{1}{2}\ln^2\frac{s}{m_Q^2} + \frac{1}{2}\ln^2\frac{\delta_s^2 s}{m_Q^2}\right. \\
&\quad \left. + \ln\frac{\psi_k^2}{4m_Q^2 s}\ln\frac{\delta_s^2 s}{m_Q^2} + 2\,\mathrm{Li}_2\left(\frac{\psi_k + 4m_Q^2}{4m_Q^2}\right) - 2\,\mathrm{Li}_2\left(\frac{-\xi_k}{\psi_k}\right) - \frac{\pi^2}{4}\right], \\
I_{0,k=3\,\text{or}\,4} &= \frac{1}{16} C_\epsilon \left[\frac{1}{\epsilon^2} - \frac{1}{\epsilon}\ln\frac{\delta_s^2 s^2}{4m_Q^4} + \frac{1}{2}\ln^2\frac{\delta_s^2 s^2}{4m_Q^4} + 2\,\mathrm{Li}_2\left(\frac{4m_Q^2 - s}{4m_Q^2}\right) - \frac{\pi^2}{4}\right], \\
I_{i=1\,\text{or}\,2,k=1\,\text{or}\,2} &= \frac{1}{8\pi^2} C_\epsilon \left[\frac{1}{\epsilon^2} - \frac{1}{\epsilon}\ln\frac{\delta_s^2 s}{m_Q^2} + \frac{1}{2}\ln^2\frac{\delta_s^2 s}{m_Q^2} - \frac{\pi^2}{4}\right], \\
I_{i=1\,\text{or}\,2,k=3\,\text{or}\,4} &= \frac{1}{8\pi^2} C_\epsilon \left[\frac{1}{\epsilon^2} - \frac{1}{\epsilon}\ln\frac{-\delta_s^2 s\xi_i}{(s-4m_Q^2)m_Q^2} + \frac{1}{2}\ln^2\frac{-\delta_s^2 s\xi_i}{(s-4m_Q^2)m_Q^2}\right. \\
&\quad \left. + \mathrm{Li}_2\left(\frac{-\psi_i + 4m_Q^2}{s-4m_Q^2}\right) - \frac{\pi^2}{4}\right], \qquad (22)
\end{aligned}$$

with $\psi_i = -2p_0 \cdot p_i$, $\xi_i = -2p_{(34)} \cdot p_i$, and $p_{(34)} = p_3 + p_4 - p_j$.

3.3 Soft part: S_2 terms

The integral of the S_2 terms in Eq. (5) over the soft phase space region is

$$\int_{p_j \text{ soft}} d\text{PS}_{p_j} S_2(n,m,p_j) = 4g_s^2 \epsilon_\beta(m_l) \sum_{\substack{i=1 \\ i\neq j}}^{4} \langle n, \text{Born}|\mathbf{T}_i(\mathbf{T}_Q - \mathbf{T}_{\overline{Q}})|m, \text{Born}\rangle \times \underbrace{\int_{p_j \text{ soft}} d\text{PS}_{p_j} \left(-\frac{p_i^\beta}{p_i \cdot p_j \; p_0 \cdot p_j} + \frac{p_0 \cdot p_i \; p_j^\beta}{p_i \cdot p_j (p_0 \cdot p_j)^2} - \frac{p_0^2 p_j^\beta}{(p_0 \cdot p_j)^3} \right)}_{=\Omega_{i,j}^\beta} . \tag{23}$$

To evaluate the phase space integrals involving p_j^β, we use the tensor decomposition

$$\int d\text{PS}_{p_j} \left(\frac{p_0 \cdot p_i}{p_i \cdot p_j (p_0 \cdot p_i)^2} - \frac{p_0^2}{(p_0 \cdot p_j)^3} \right) p_j^\beta = \begin{cases} A_1 p_i^\beta + A_2 p_{(34)}^\beta + A_3 p_0^\beta & \text{for } i = 1,2 \\ A_4 p_{(34)}^\beta + A_5 p_0^\beta & \text{for } i = 3,4 \end{cases} , \tag{24}$$

which leads to the expressions

$$\begin{aligned}
\Omega_{i=1\text{ or }2,j}^\beta = p_i^\beta \int_{p_j \text{ soft}} d\text{PS}_{p_j} \Bigg[& \frac{\left(s - 4m_Q^2\right)\left(\psi_i s + 4m_Q^2(s + 3\xi_i)\right)}{2\left(\psi_i + 4m_Q^2\right) s\xi_i} \frac{1}{(p_0 \cdot p_j)^2} \\
& - \frac{\psi_i s - 4m_Q^2(\psi_i + 2\xi_i)}{2\left(\psi_i + 4m_Q^2\right) s} \frac{1}{p_i \cdot p_j \; p_0 \cdot p_j} + \frac{4m_Q^2\left(\psi_i s + 4m_Q^2(s - \xi_i)\right)}{\left(\psi_i + 4m_Q^2\right) s\xi_i} \frac{p_3 \cdot p_4}{(p_0 \cdot p_j)^3} \\
& + \frac{4m_Q^2\left(s - 4m_Q^2\right)^2}{\left(\psi_i + 4m_Q^2\right) s\xi_i} \frac{p_i \cdot p_j}{(p_0 \cdot p_j)^3} + \frac{\psi_i\left(\psi_i s - 4m_Q^2(\psi_i + 2\xi_i)\right)}{2\left(\psi_i + 4m_Q^2\right) s\xi_i} \frac{p_3 \cdot p_4}{(p_0 \cdot p_j)^2 \; p_i \cdot p_j} \Bigg] \\
& + p_{(34)}^\beta \int_{p_j \text{ soft}} d\text{PS}_{p_j} \Bigg[\frac{4m_Q^2 \psi_i^2}{\left(\psi_i + 4m_Q^2\right) s\xi_i} \frac{p_3 \cdot p_4}{(p_0 \cdot p_j)^3} - \frac{\psi_i^2}{2\left(\psi_i + 4m_Q^2\right) s} \frac{1}{p_0 \cdot p_j \; p_i \cdot p_j} \\
& + \frac{4\left(\psi_i s m_Q^2 - 4m_Q^4(\psi_i + 2\xi_i)\right)}{\left(\psi_i + 4m_Q^2\right) s\xi_i} \frac{p_i \cdot p_j}{(p_0 \cdot p_j)^3} + \frac{\psi_i^3}{2\left(\psi_i + 4m_Q^2\right) s\xi_i} \frac{p_3 \cdot p_4}{(p_0 \cdot p_j)^2 \; p_i \cdot p_j} \\
& + \frac{\psi_i\left(\psi_i s - 4m_Q^2(\psi_i + 4\xi_i)\right)}{2\left(\psi_i + 4m_Q^2\right) s\xi_i} \frac{1}{(p_0 \cdot p_j)^2} \Bigg] + \left(p_0^\beta \text{ terms} \right) , \\
\Omega_{i=3\text{ or }4,j}^\beta = p_{(34)}^\beta \int_{p_j \text{ soft}} d\text{PS}_{p_j} & \left(-\frac{2p_0^2}{(p_0 \cdot p_j)^2 \; p_0 \cdot p_j} + \frac{\left(p_0^2\right)^2 \; p_i \cdot p_j}{(p_0 \cdot p_j)^3 (p_0 \cdot p_i)^2} \right) + \left(p_0^\beta \text{ terms} \right) ,
\end{aligned} \tag{25}$$

where the p_0^β terms vanish upon contraction with $\epsilon_\beta(m_l)$ in Eq. (23). As for $\Omega_{i=1\text{ or }2,j}$, the angular integrals needed to evaluate $\int_{p_j \text{ soft}} p_i \cdot p_j / (p_0 \cdot p_j)^3$ and $\int_{p_j \text{ soft}} p_3 \cdot p_4 / ((p_0 \cdot p_j)^2 (p_i \cdot p_j))$ are not listed in Ref. [4] or the references cited therein. We obtain these by relating the

phase space integrals to cut virtual-correction loop integrals and evaluating the latter by means of the integration-by-parts technique [9]. The final results are

$$\begin{aligned}
\Omega^{\beta}_{i=1\,\text{or}\,2,j} = &-\frac{C_\epsilon p_i^\beta}{4\pi^2\psi_i}\left[\frac{1}{\epsilon} - \frac{\psi_i^2+\psi_i\xi_i+4m_Q^2(\psi_i+2\xi_i)}{\xi_i\left(\psi_i+4m_Q^2\right)}\ln\frac{-\psi_i}{4m_Q^2} - \frac{s}{\xi_i}\ln\frac{s}{4m_Q^2} - \ln\frac{\delta_s^2 s}{m_Q^2}\right] \\
&- \frac{p^\beta_{(34)}}{4\pi^2\xi_i}\left[\frac{\left(s^2-16m_Q^4\right)\xi_i}{\left(s-4m_Q^2\right)^3} + \frac{\psi_i}{\psi_i+4m_Q^2}\ln\frac{-\psi_i}{4m_Q^2}\right. \\
&\left. + \frac{16m_Q^4\psi_i + s^2\left(\psi_i+8m_Q^2\right)}{\left(s-4m_Q^2\right)^3}\ln\frac{s}{4m_Q^2}\right] + \left(p_0^\beta\,\text{terms}\right), \\
\Omega^{\beta}_{i=3\,\text{or}\,4,j} = &\frac{C_\epsilon p^\beta_{(34)}}{4\pi^2(s-4m_Q^2)}\left[\frac{1}{\epsilon}+1-\frac{2s}{s-4m_Q^2}+\frac{2s^2}{\left(s-4m_Q^2\right)^2}\ln\frac{s}{4m_Q^2} - \ln\frac{\delta_s^2 s^2}{4m_Q^4}\right] \\
&+ \left(p_0^\beta\,\text{terms}\right).
\end{aligned} \tag{26}$$

3.4 Soft part: S_3 terms

The integral of the S_3 terms in Eq. (6) over the soft phase space region is

$$\begin{aligned}
\int_{p_j\,\text{soft}} d\text{PS}_{p_j} S_3(m,p_j) = &\, 4g_s^2\epsilon^*_\alpha(m_l)\epsilon_\beta(m_l)\langle m,\text{Born}|(\mathbf{T}_Q-\mathbf{T}_{\overline{Q}})(\mathbf{T}_Q-\mathbf{T}_{\overline{Q}})|m,\text{Born}\rangle \\
&\times \underbrace{\int_{p_j\,\text{soft}} d\text{PS}_{p_j}\left(-\frac{g^{\alpha\beta}}{(p_0\cdot p_j)^2} - \frac{p_0^2\,p_j^\alpha p_j^\beta}{(p_0\cdot p_j)^4}\right)}_{=\Omega_j^{\alpha\beta}}.
\end{aligned} \tag{27}$$

To evaluate the integral involving $p_j^\alpha p_j^\beta$, we use the tensor decomposition

$$\int d\text{PS}_{p_j}\frac{p_j^\alpha p_j^\beta}{(p_0\cdot p_j)^4} = A_6 g^{\alpha\beta} + A_7 p^\alpha_{(34)}p^\beta_{(34)} + A_8 p_0^\alpha p_0^\beta + A_9\left(p_0^\alpha p^\beta_{(34)} + p^\alpha_{(34)}p_0^\beta\right), \tag{28}$$

resulting in

$$\begin{aligned}
\Omega_j^{\alpha\beta} = &\frac{g^{\alpha\beta}}{\epsilon-1}\int_{p_j\,\text{soft}} d\text{PS}_{p_j}\left[\frac{32m_Q^4}{\left(s-4m_Q^2\right)^2}\frac{(p_3\cdot p_4)^2}{(p_0\cdot p_j)^4} - \frac{8m_Q^2}{s-4m_Q^2}\frac{p_3\cdot p_4}{(p_0\cdot p_j)^3} - \frac{\epsilon-1}{(p_0\cdot p_j)^2}\right] \\
&+ \frac{16p^\alpha_{(34)}p^\beta_{(34)}}{\epsilon-1}\int_{p_j\,\text{soft}} d\text{PS}_{p_j}\left[\frac{32(3-2\epsilon)m_Q^6}{\left(s-4m_Q^2\right)^4}\frac{(p_3\cdot p_4)^2}{(p_0\cdot p_j)^4} - \frac{(\epsilon-1)m_Q^2}{\left(s-4m_Q^2\right)^2}\frac{1}{(p_0\cdot p_j)^2}\right. \\
&\left. - \frac{8(3-2\epsilon)m_Q^4}{\left(s-4m_Q^2\right)^3}\frac{p_3\cdot p_4}{(p_0\cdot p_j)^3}\right] + (p_0\,\text{terms}),
\end{aligned} \tag{29}$$

where the p_0^α and p_0^β terms vanish upon contraction with $\epsilon_\beta(m_l)$ in Eq. (27). Evaluating the integrals analytically and adding the corresponding operator renormalization counterterm contribution of Eqs. (10) or (12), we arrive at the finite expression

$$\begin{aligned}\left(\Omega_j^{\alpha\beta}\right)_{+\text{op. ren.}} = \frac{g^{\alpha\beta}}{48m_Q^2\pi^2}\Bigg[&-\frac{\left(s+4m_Q^2\right)^2}{2\left(s-4m_Q^2\right)^2}-\frac{1}{2}\ln\frac{4\delta_s^4 s}{m_Q^2}-\ln\frac{m_Q^2}{\mu_\Lambda^2}\\ &+\left(\frac{2s^3}{\left(s-4m_Q^2\right)^3}-\frac{3s^2}{\left(s-4m_Q^2\right)^2}+\frac{6m_Q^2}{s-4m_Q^2}+\frac{3s}{2\left(s-4m_Q^2\right)}\right)\ln\frac{s}{4m_Q^2}\Bigg]\\ &+\frac{p_{(34)}^\alpha p_{(34)}^\beta}{\pi^2}\Bigg[-\frac{2s^2}{\left(s-4m_Q^2\right)^4}+\frac{2s}{\left(s-4m_Q^2\right)^3}-\frac{1}{6\left(s-4m_Q^2\right)^2}\\ &+\frac{2s^3-3s^2\left(s-4m_Q^2\right)+s\left(s-4m_Q^2\right)^2}{\left(s-4m_Q^2\right)^5}\ln\frac{s}{4m_Q^2}\Bigg]+(p_0\,\text{terms})\,. \end{aligned} \tag{30}$$

3.5 A remark on the tensor decomposition

We note that the tensor decompositions of Eqs. (24) and (28) involve momentum $p_{(34)}$. A potential pitfall is that $p_{(34)}$ does not appear in the integrand of Eq. (28), nor does it in Eq. (24) in the cases $i = 1$ or 2, and one might naïvely think that $d\text{PS}_{p_j}$ only involves momentum p_j, of which $p_{(34)}$ is independent in the limit of p_j being soft. Thus, one might be led to assume that the structures with $p_{(34)}$ are not necessary in the above-mentioned cases. Using a tensor decomposition with the $p_{(34)}$ structures omitted then leads to incorrect results for $\Omega^\beta_{i=1\,\text{or}\,2,j}$ and $\Omega_j^{\alpha\beta}$. Incidentally, this does not spoil the the infrared finiteness, which would have served as a crucial check otherwise. So, this mistake is easily made and more easily overlooked. As already mentioned in Ref. [12], Ref. [11] is affected by this mistake. The numerical effects of this are discernible in Fig. 2 of Ref. [11], where the dashed curves, indicating the ${}^3P_J^{[8]}$ contributions, are subject to visible deviations. Fortunately, the effects on the physical results in Fig. 1 of Ref. [11] are insignificant, being of the order of the numerical uncertainty. We believe that this easy-to-miss mistake has also creeped into other authors' calculations. In fact, Eqs. (5) and (6) of Ref. [13] only hold if the incorrect tensor decomposition is applied. Furthermore, purposely including this mistake, we are able to approximately reproduce the results shown in Fig. 3 of Ref. [14] and Fig. 2 of Ref. [15], while our correct evaluations significantly differ from these results.

4 Dipole subtraction implementation

4.1 Summary of dipole subtraction formalism

Our implementation of dipole subtraction, which is based on Refs. [6,8] is explained in detail in Ref. [7]. For the reader's convenience, we recall the main formulas here. We

calculate the NLO corrections to our partonic cross sections as

$$\begin{aligned}\int d\hat{\sigma} = \int d\mathrm{PS}_3 \left[\frac{d\hat{\sigma}_{\mathrm{real}}}{d\mathrm{PS}_3}\theta(p_T - p_{T,\mathrm{min}}) - \frac{d\hat{\sigma}_{\mathrm{subtr}}}{d\mathrm{PS}_3}\theta(\tilde{p}_T - p_{T,\mathrm{min}})\right] \\ + \int d\mathrm{PS}_2 \left[\frac{d\hat{\sigma}_{\mathrm{virtual}} + d\hat{\sigma}_{\mathrm{MFC}} + d\hat{\sigma}_{\mathrm{op.\,ren.}}}{d\mathrm{PS}_2}\theta(p_T - p_{T,\mathrm{min}})\right. \\ \left. + [dx]\theta(\tilde{p}_T - p_{T,\mathrm{min}}) \int d\mathrm{PS}_{\mathrm{dipole}} \frac{d\hat{\sigma}_{\mathrm{subtr}}}{d\mathrm{PS}_3}\right], \end{aligned} \tag{31}$$

where $d\mathrm{PS}_2$ and $d\mathrm{PS}_3$ are the two- and three-particle phase space factors. The latter factorize in some way as $d\mathrm{PS}_2 d\mathrm{PS}_{\mathrm{dipole}}$ or $d\mathrm{PS}_2 dx d\mathrm{PS}_{\mathrm{dipole}}$, where dx matches its counterpart in Eq. (9). $d\hat{\sigma}_{\mathrm{real}}$, $d\hat{\sigma}_{\mathrm{virtual}}$, $d\hat{\sigma}_{\mathrm{MFC}}$, and $d\hat{\sigma}_{\mathrm{op.\,ren.}}$ are the real-correction contributions, the virtual-correction contributions, the mass factorization counterterms, and operator renormalization counterterms, respectively. The *subtraction term* $d\hat{\sigma}_{\mathrm{subtr}}$ is given by

$$\begin{aligned}\frac{d\hat{\sigma}_{\mathrm{subtr}}(a+b \to Q\overline{Q}[n] + X)}{d\mathrm{PS}_3} = \frac{1}{N_{\mathrm{col}}(n) N_{\mathrm{pol}}(n)} \frac{1}{2(p_1+p_2)^2} \\ \times \frac{F_{\mathrm{sym}}(X)}{n_{\mathrm{col}}(a) n_{\mathrm{pol}}(a) n_{\mathrm{col}}(b) n_{\mathrm{pol}}(b)} \| |abn, \mathrm{subtr}\rangle \|^2, \end{aligned} \tag{32}$$

with

$$\begin{aligned}\| |abn, \mathrm{subtr}\rangle \|^2 = \sum_{j=3}^{4} \sum_{i=1}^{2} \sum_{\substack{k=0 \\ k\neq i,j}}^{4} \frac{n_{\mathrm{col}}(i)}{n_{\mathrm{col}}((ij))} \frac{-1}{2p_i \cdot p_j} \frac{1}{x} \langle n, \mathrm{Born}| V_{ij,k}^{\mathrm{ini},S_1} \frac{\mathbf{T}_{(ij)}\mathbf{T}_k}{\mathbf{T}_{(ij)}^2} |n, \mathrm{Born}\rangle \\ + \sum_{j=3}^{4} \sum_{\substack{i=0 \\ i\neq 1,2,j}}^{3} \sum_{\substack{k=0 \\ k\neq i,j}}^{4} \frac{-1}{2p_i \cdot p_j} \langle n, \mathrm{Born}| V_{ij,k}^{\mathrm{fin},S_1} \frac{\mathbf{T}_{(ij)}\mathbf{T}_k}{\mathbf{T}_{(ij)}^2} |n, \mathrm{Born}\rangle \begin{cases} \frac{1}{x} & \text{if } k = 1,2 \\ 1 & \text{if } k \neq 1,2 \end{cases} \\ + \sum_{j=3}^{4} \sum_{\substack{i=1 \\ i\neq j}}^{4} V_{S_2,ij}^{\beta} \epsilon_\beta(m_l) \langle n, \mathrm{Born}| \mathbf{T}_{(ij)}(\mathbf{T}_Q - \mathbf{T}_{\overline{Q}}) |m(n), \mathrm{Born}\rangle \\ + \sum_{j=3}^{4} V_{S_3,j}^{\alpha\beta} \epsilon_\alpha^*(m_l) \epsilon_\beta(m_l) \langle m(n), \mathrm{Born}| (\mathbf{T}_Q - \mathbf{T}_{\overline{Q}})(\mathbf{T}_Q - \mathbf{T}_{\overline{Q}}) |m(n), \mathrm{Born}\rangle. \end{aligned} \tag{33}$$

This term is defined in terms of $2 \to 3$ kinematic variables in the same way as $d\hat{\sigma}_{\mathrm{real}}$ and constructed so that it matches $d\hat{\sigma}_{\mathrm{real}}$ in all singular limits: We call each term in the sum a *dipole*. The dipoles in the first and second lines of Eq. (33) reproduce $d\hat{\sigma}_{\mathrm{real}}$ in the initial- and final-state collinear limits as well as the S_1 part of the soft limits, while the dipoles in the last two lines reproduce the S_2 and S_3 parts of the soft limits. As for the Born amplitudes in Eq. (33), partons i and j are replaced by (ij), which is a gluon, light quark, or the $Q\overline{Q}$ pair, according to the soft or collinear limits to be approximated.

The contribution in Eq. (32) is set to zero if there is no collinear or soft singularity in the considered limit. In the dipoles for the S_2 and S_3 terms, $m({}^3P_J^{[1/8]}) = {}^3S_1^{[1/8]}$ and $m({}^1P_1^{[1/8]}) = {}^1S_0^{[1/8]}$. Since the Born amplitudes are defined in terms of $2 \to 2$ kinematic variables, we need for each dipole a *mapping* of the $2 \to 3$ process momenta to $2 \to 2$ kinematics momenta $\tilde{p}_i$. These momentum mappings are constructed in such a way that the Born amplitudes in Eq. (33) equal their counterparts in the factorization formulae of the respective collinear and soft limits. Furthermore, we define

$$\tilde{p}_T^2 = \frac{(4m_Q^2 - \tilde{t})(\tilde{s} + \tilde{t})}{\tilde{s}} - 4m_Q^2, \qquad \tilde{y} = \ln \frac{\tilde{s} + \tilde{t}}{\tilde{x}_2 \sqrt{S\left(\tilde{p}_T^2 + 4m_Q^2\right)}}, \tag{34}$$

with

$$\tilde{s} = (\tilde{p}_1 + \tilde{p}_2)^2, \qquad \tilde{t} = (\tilde{p}_0 - \tilde{p}_1)^2, \qquad S = (p_A + p_B)^2, \qquad \tilde{p}_2 = \tilde{x}_2 p_B, \tag{35}$$

where p_A and p_B are the momenta of the incoming hadrons.

The idea of the subtraction formalism is that the term in the first square bracket of Eq. (31) is devoid of singularities and can, therefore, be integrated over numerically in four dimensions. On the other hand, the various V terms in Eq. (33) are defined only in terms of those kinematic variables that we use to parametrize $d\mathrm{PS}_{\mathrm{dipole}}$, and are sufficiently simple to be integrated analytically over $d\mathrm{PS}_{\mathrm{dipole}}$. The resulting poles in ϵ then render the second square bracket in Eq. (33) finite and ready for numerical integration over $d\mathrm{PS}_2$ and dx.

In practice, we need to produce predictions involving experimental cuts on the transverse momentum p_T and the rapidity y of the heavy quarkonium, see for example the low-p_T cut in Eq. (31). The implementation of these phase space cuts is, however, unproblematic, too, since, in the first square bracket of Eq. (31), p_T and $\tilde{p}_T$ coincide in the singular limits and, in the second square bracket, the θ function stands outside the analytic $d\mathrm{PS}_{\mathrm{dipole}}$ integration.

Table 1 indicates where one can find the analytic expressions for the various V terms, their counterparts upon integration over the respective phase space $d\mathrm{PS}_{\mathrm{dipole}}$, and their respective momentum mappings. As for the V terms of the Catani-Seymour [6] and Phaf-Weinzierl [8] papers, $V_{ij,k}^{\mathrm{ini},S_1}$ equals V_k^{ij} or $V^{ij,k}$ and $V_{ij,k}^{\mathrm{fin},S_1}$ equals $V_{ij,k}$ or V_{ij}^k in their notations. Indices s and s' or μ and ν within $V_{ij,k}$ are to be contracted with the open polarization indices of particle (ij) in the corresponding Born amplitude. Figure 1 summarizes all dipole terms according to their corresponding singular limits in a graphical form.

4.2 Organization in terms of computer codes

In this section, we briefly describe how we implement the dipole subtraction procedure in our computer codes, emphasizing those parts which differ from our implementation of phase space slicing. All necessary Born diagrams are created with `FeynArts` and then treated by a Mathematica script which inserts the color operators $\mathbf{T}$ in the various combinations needed and applies the color-singlet and color-octet projectors to evaluate all color

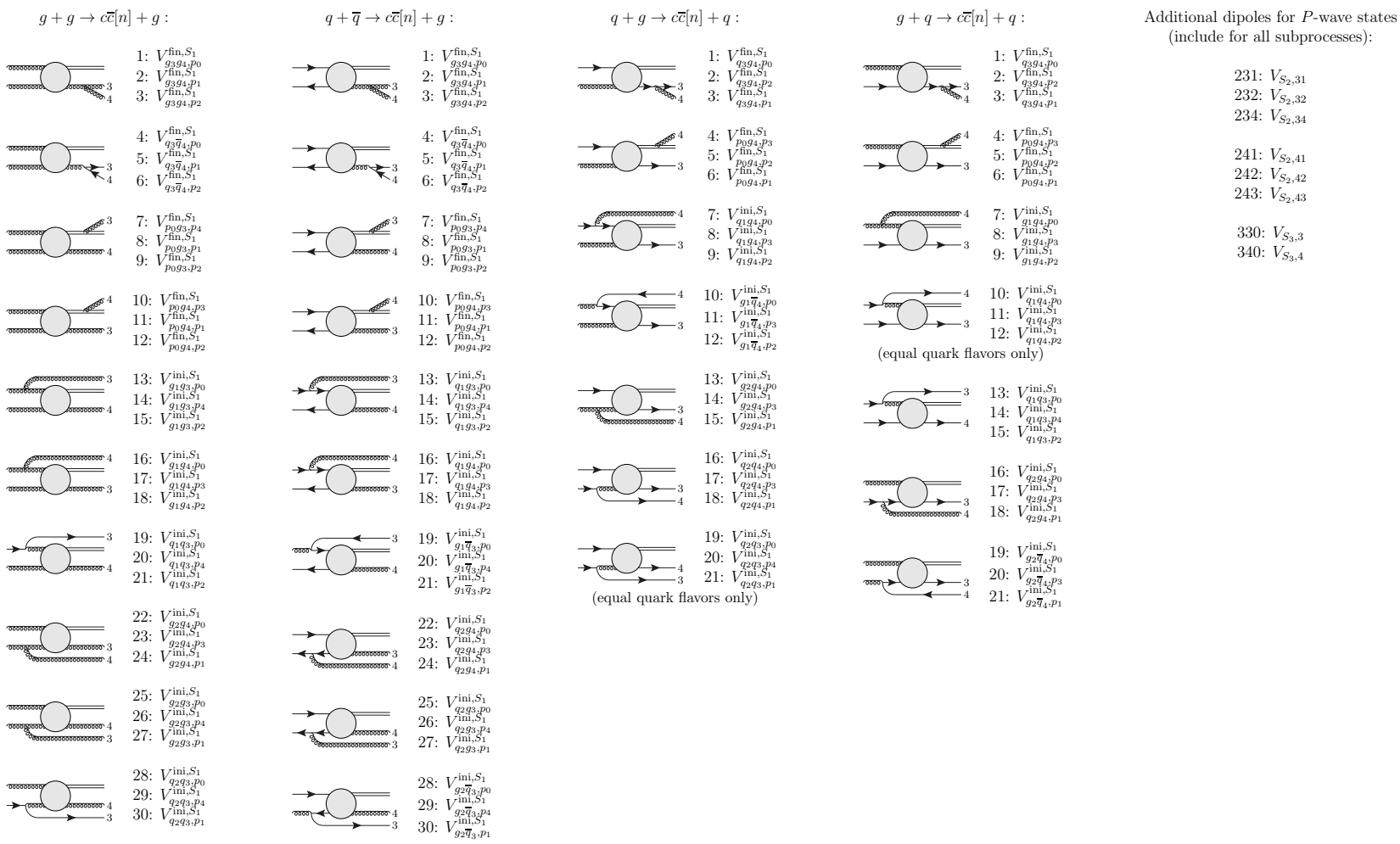

Figure 1: Numbered list of dipole terms for each of the occurring Born processes with $2 \to 2$ kinematics. The diagrams related to the $V^{\mathrm{ini},S_1}_{ij,k}$ and $V^{\mathrm{fin},S_1}_{ij,k}$ terms indicate in which collinear or soft limits the latter contribute. Light-quark lines are to be summed over all quark flavors.

	p_i	p_k	Definition and Integration	Applied Mapping
$V_{ij,k}^{\text{ini},S_1}$	p_1 or p_2	p_0	PW, section 6.1	MapPW6(p_i, p_j)
$V_{ij,k}^{\text{ini},S_1}$	p_1 or p_2	p_1 or p_2	CS, section 5.6 ($n = p_3 + p_4$)	MapCS(p_i)
$V_{ij,k}^{\text{ini},S_1}$	p_1 or p_2	p_3 or p_4	CS, section 5.3	MapCS(p_i)
$V_{ij,k}^{\text{fin},S_1}$	p_0	p_1 or p_2	PW, section 6.2	MapPW6(p_k, p_j)
$V_{ij,k}^{\text{fin},S_1}$	p_0	p_3 or p_4	PW, section 5.2	MapPW5.2(p_j)
$V_{ij,k}^{\text{fin},S_1}$	p_3 or p_4	p_0	PW, section 5.1	MapPW5.1(p_i)
$V_{ij,k}^{\text{fin},S_1}$	p_3 or p_4	p_1 or p_2	CS, section 5.2	MapCS(p_k)
$V_{S_2,ij}$	p_1 or p_2		BK, (75) and section 4.5.1	MapPW6(p_i, p_j)
$V_{S_2,ij}$	p_3 or p_4		BK, (75) and section 4.5.2	MapPW5.2(p_j)
$V_{S_3,j}$			BK, (76) and section 4.5.3	MapPW5.2(p_j)

Table 1: List of occurring V terms with given momentum assignments; of where their definitions and analytic expressions upon integration over the dipole phase spaces may be found in the Catani-Seymour (CS) [6], Phaf-Weinzierl (PW) [8], and Butenschoen-Kniehl (BK) [7] papers; and of momentum mappings, according to the naming scheme of Ref. [7], to be applied to the numerical integrations of the respective dipole terms over $d\text{PS}_3$.

factors in the squared amplitudes. These color factors, together with the yet unsquared amplitudes, are then passed to two FORM scripts, `CalcDipoles` and `CalcDipolesInteg`. For these two routines, we have prepared an input card which encodes the information of Figure 1.

`CalcDipoles` generates the FORTRAN routines encoding the dipole terms. This is done by squaring the Born amplitudes, written in terms of the $\tilde{p}_i$ momenta and with the respective color insertions, and multiplying them by the necessary factors, in particular $V_{ij,k}$, taking into account the spin correlations in the case of splitting gluons. Then, the respective momentum mappings are implemented, the resulting expressions are simplified, and the FORTRAN routine `AMP2_Dipoles` is generated, which takes as arguments the number of the dipole and the partonic $2 \to 3$ kinematic variables.

Similarly, `CalcDipolesInteg` squares the Born amplitudes with the respective color insertions, and then multiplies the finite parts of the V terms integrated over the dipole phase space $d\text{PS}_{\text{dipole}}$. At this point, the mass factorization and operator renormalization counterterms are included, as described in Ref. [7]. The integrated dipoles have the general form $[h(x)]_+ f(x) + g(x)$, where $h(x)$ is singular in the limit $x \to 1$. The generated FORTRAN function `AMP2_DipolesInteg` takes as arguments the number of the dipole, the $2 \to 2$ kinematics variables, and the value of x. A second function, `AMP2_Dipoles-IntegSubtr`, which only contains the terms $h(x)f(1)$, is generated as well.

Together with the FORTRAN functions for the virtual- and the real-correction squared amplitudes, we then have the ingredients for the numerical phase space integrations in the main FORTRAN code. The θ functions constraining the $2 \to 3$ particle phase space in Eq. (31) have to be implemented for each dipole individually with the respective mo-

mentum mapping. The x integrations over the plus distributions are thereby explicitly implemented as

$$\int_{x_{\min}}^{1} dx \Big\{ [h(x)]_+ f(x) + g(x) \Big\} = \int_0^1 dx \Big\{ \theta(x - x_{\min}) \underbrace{\big[h(x) f(x) + g(x) \big]}_{\texttt{AMP2\_DipolesInteg}} - \underbrace{h(x) f(1)}_{\substack{\texttt{AMP2\_Dipoles} \\ \texttt{IntegSubtr}}} \Big\}, \tag{36}$$

so that the singularities of the $h(x)$ terms for $x \to 1$ cancel numerically in the course of the integration.

4.3 Numerical tests of the integrated dipole terms

In Ref. [7], we have already described one numerical test of our dipole subtraction implementation, namely we have shown that our expressions for the dipole terms agree with the real-correction contributions in the corresponding singular limits. Here, we describe a further internal test. This time, we test the expressions of the integrated dipole terms. We do this by evaluating the phase space integrals,

$$\mathcal{I}_i = \int d\mathrm{PS}_3 \theta(p_T - p_{T,\min}) \left(\| |abn, \mathrm{subtr} \rangle_{\mathrm{dipole}\, i} \|^2 \right)_{+\mathrm{MFC}\, +\mathrm{op.\,ren.}}, \tag{37}$$

of specific dipole terms plus the corresponding mass factorization and operator renormalization counterterms in two different ways and comparing the results. In the first mode of evaluation, we use the results of the expressions implemented in `CalcDipolesInteg` and integrate them numerically over $d\mathrm{PS}_2$ or $d\mathrm{PS}_2 dx$. In the second mode of evaluation, we separate the three-particle phase space as in the phase space slicing implementation according to the slicing parameters δ_s and δ_c. For the contributions from the soft and collinear regions, we take the respective analytic limits of the dipole terms, integrate them analytically over the corresponding phase space, $d\mathrm{PS}_{p_j\,\mathrm{soft}}$ or $d\mathrm{PS}_{i\|j}$, add the corresponding mass factorization and operator renormalization counterterms, and then do the integrations over $d\mathrm{PS}_2$ or $d\mathrm{PS}_2 dx$ numerically. For the contribution from the hard-noncollinear region, we integrate the expressions for the dipole terms as encoded in `CalcDipoles` numerically over $d\mathrm{PS}_3$. Both contributions are then combined to yield the final results of the second mode of evaluation. We perform these tests with groups of one, two, or three dipoles in order to simplify the analytic integrations of the soft limits in the second version. We have successfully tested all the dipoles in this way. Typical examples are presented in Table 2.

5 Comparison of phase space slicing and dipole subtraction methods

In Tables 3–6, we compare our dipole subtraction and phase space slicing implementations. We calculate at NLO total cross sections, including the Born contributions, of inclusive

```
DipoleIntegtest gg2cCg for State 3PJ8.
Dipole  8 on.
Dipole 13 on.

 Result Analytic:    20193.01298070771 ± 2.996135930530795

 Result Slicing:
  0.000001      -1.4614E+05 ± 1.0517E+01     1.6171E+05 ± 8.8167E+02     1.5567E+04 ± 8.8173E+02
  0.000010      -1.0832E+05 ± 8.3362E+00     1.2746E+05 ± 3.4805E+02     1.9130E+04 ± 3.4815E+02
  0.000100      -7.4543E+04 ± 5.6847E+00     9.4589E+04 ± 2.0637E+02     2.0047E+04 ± 2.0644E+02
  0.001000      -4.4854E+04 ± 3.6687E+00     6.4916E+04 ± 8.2790E+01     2.0063E+04 ± 8.2871E+01
  0.010000      -1.9291E+04 ± 1.7919E+00     3.9340E+04 ± 3.2753E+01     2.0049E+04 ± 3.2802E+01


DipoleIntegtest gd2cCd for State 3P21.
Dipole 243 on.

 Result Analytic:   -170.1669990971855 ± 1.5578494469294161E-004

 Result Slicing:
  0.000001       4.5608E+02 ± 4.0023E-04    -6.2616E+02 ± 2.3290E-01    -1.7008E+02 ± 2.3290E-01
  0.000010       3.6877E+02 ± 3.2966E-04    -5.3970E+02 ± 2.0804E-01    -1.7093E+02 ± 2.0804E-01
  0.000100       2.8332E+02 ± 2.7631E-04    -4.5313E+02 ± 1.4900E-01    -1.6981E+02 ± 1.4900E-01
  0.001000       1.9636E+02 ± 1.9533E-04    -3.6631E+02 ± 1.1489E-01    -1.6995E+02 ± 1.1489E-01
  0.010000       1.0978E+02 ± 1.0843E-04    -2.7811E+02 ± 7.8774E-02    -1.6833E+02 ± 7.8774E-02
```

Table 2: Numerical tests of integrated dipole subtraction terms as described in Section 4.3. The finite parts of I_i in Eq. (37) are evaluated for $g + g \to c\bar{c}[^3P_J^{[8]}] + g$ with dipoles 8 and 13 and for $g + d \to c\bar{c}[^3P_J^{[8]}] + d$ with dipole 243 using the implementations of dipole subtraction and phase space slicing, for $n_f = 3$, $\alpha_s = 1/(4\pi)$, $\mu_f = 0.5$ GeV, $m_Q = 0.2$ GeV, $(p_1 + p_2)^2 = 100$ GeV^2, $p_{T,\min} = 2$ GeV, $\delta_c = \delta$, and $\delta_s = \delta/1000$ with variable value of δ. For a given value of δ (first column), the soft and collinear parts (second column), the hard-noncollinear parts (third column), and their sum (forth column) are listed. The quoted errors are the numerical-integration uncertainties.

charmonium production in proton-antiproton collisions at typical center-of-mass-energies for selected bins of transverse momentum and rapidity. As in Refs. [10,11,12], we treat the first $n_f = 3$ quark flavors as massless, take the heavy-quark mass, defined in the on-shell renormalization scheme, to be $m_Q = 1.5$ GeV, use set CTEQ6M [16] of proton PDFs, evaluate $\alpha_s = \alpha_s^{(4)}(\mu_r)$ at two loops with asymptotic scale parameter $\Lambda_{\rm QCD}^{(4)} = 326$ MeV [16], and choose the renormalization and factorizations scales to be $\mu_r = \mu_f = \sqrt{p_T^2 + 4m_Q^2}$ and $\mu_\Lambda = m_Q$. For definiteness, we set $\langle \mathcal{O}^H({}^3S_1^{[8]}) \rangle = 1$ GeV^3 and $\langle \mathcal{O}^H({}^3P_0^{[1]}) \rangle = 1$ GeV^5. In the phase space slicing implementation, we choose the cut-off parameters to be $\delta_s = \delta$ and $\delta_c = \delta/1000$, vary δ from 10^{-6} to 10^{-2}, and take the evaluation with $\delta = 10^{-3}$ as default to be compared with the results obtained using dipole subtraction.

From Tables 3–6, we observe that the results obtained in the selected bins using the two implementations numerically agree at the level of about 10%, in line with the uncertainty inherent in the application of the phase space slicing method. Besides being more accurate, the dipole subtraction implementation is also typically much faster than the phase space slicing implementation. The reason for that is that, in the phase space slicing implementation, there is usually a much stronger numerical cancellation between the contributions from the analytic and numerical integrations than in the dipole subtraction implementation, necessitating a higher relative accuracy in the numerical integrations. However, this advantage is to some extent compensated by the fact that the θ functions in the first term of Eq. (31) cut out very different phase space regions and so worsen the convergence of the numerical Monte-Carlo integrations in the dipole subtraction implementation. Nevertheless, we observe that our dipole implementation achieves a final accuracy of 1% typically 2 to 6 times faster than the phase space slicing implementation.

6 Summary

In this article, we have reviewed the singularity structure of NLO NRQCD calculations of the production of heavy-quark pairs in S and P wave states and provided details of our phase space slicing implementation thereof. Thereby, we have identified a common mistake in the literature. Furthermore, we have summarized the dipole subtraction formalism for such calculations, which we have recently developed in Ref. [7], added details about its implementation in terms of computer codes, and performed internal numeric tests. Finally, we have extensively compared our two implementations numerically and found reasonable agreement. As expected, the dipole subtraction implementation outperforms the phase space slicing implementation both with regard to accuracy and speed.

Acknowledgments

We would like to thank Anatoly Kotikov for assistance in evaluating a particular Feynman diagram. This work was supported in part by the German Federal Ministry for Education

p+$\bar{\text{p}}$ --> c$\bar{\text{c}}$[3S18] + X: Sqrt[s] = 100 GeV, 2 GeV < p_T < 3 GeV, -0.5 < y < 0.5:

Dipole implementation: 1.8694E+03 ± 1.8683E+00

Slicing implementation:

0.000010	-4.2106E+04 ± 1.3991E+01	4.3677E+04 ± 1.4321E+01	1.5710E+03 ± 2.0021E+01
0.000032	-3.5355E+04 ± 1.0905E+01	3.7067E+04 ± 9.5207E+00	1.7120E+03 ± 1.4477E+01
0.000100	-2.9207E+04 ± 8.8019E+00	3.0987E+04 ± 6.1790E+00	1.7800E+03 ± 1.0754E+01
0.000320	-2.3394E+04 ± 6.1821E+00	2.5209E+04 ± 3.9720E+00	1.8149E+03 ± 7.3482E+00
0.001000	-1.8171E+04 ± 4.6479E+00	1.9989E+04 ± 2.5723E+00	1.8184E+03 ± 5.3122E+00
0.003200	-1.3329E+04 ± 3.3122E+00	1.5139E+04 ± 1.6327E+00	1.8103E+03 ± 3.6927E+00
0.010000	-9.0788E+03 ± 2.1645E+00	1.0867E+04 ± 1.0867E+00	1.7882E+03 ± 2.4220E+00

Relative difference using default slicing parameter: -2.7%
Factor of time the dipole implementation is faster: 9.6

p+$\bar{\text{p}}$ --> c$\bar{\text{c}}$[3S18] + X: Sqrt[s] = 100 GeV, 6 GeV < p_T < 7 GeV, -0.5 < y < 0.5:

Dipole implementation: 2.6433E+01 ± 2.5363E-02

Slicing implementation:

0.000010	-5.9185E+02 ± 1.9436E-01	6.1327E+02 ± 3.7003E-01	2.1420E+01 ± 4.1797E-01
0.000032	-4.9661E+02 ± 1.4844E-01	5.2090E+02 ± 2.4433E-01	2.4290E+01 ± 2.8589E-01
0.000100	-4.0982E+02 ± 1.1312E-01	4.3508E+02 ± 1.0923E-01	2.5260E+01 ± 1.5725E-01
0.000320	-3.2764E+02 ± 8.2613E-02	3.5340E+02 ± 1.6469E-01	2.5761E+01 ± 1.8425E-01
0.001000	-2.5363E+02 ± 5.8880E-02	2.7997E+02 ± 2.3740E-01	2.6338E+01 ± 2.4459E-01
0.003200	-1.8482E+02 ± 4.0917E-02	2.1062E+02 ± 7.1737E-02	2.5795E+01 ± 8.2586E-02
0.010000	-1.2431E+02 ± 2.6148E-02	1.4989E+02 ± 1.9901E-01	2.5578E+01 ± 2.0072E-01

Relative difference using default slicing parameter: -0.4%
Factor of time the dipole implementation is faster: 6.4

p+$\bar{\text{p}}$ --> c$\bar{\text{c}}$[3S18] + X: Sqrt[s] = 1960 GeV, 7 GeV < p_T < 8 GeV, -0.6 < y < 0.6:

Dipole implementation: 2.3196E+03 ± 2.3170E+00

Slicing implementation:

0.000010	-6.6859E+04 ± 2.0831E+01	6.8617E+04 ± 1.7129E+02	1.7580E+03 ± 1.7255E+02
0.000032	-5.6557E+04 ± 1.5699E+01	5.8597E+04 ± 3.8898E+01	2.0400E+03 ± 4.1946E+01
0.000100	-4.7142E+04 ± 1.2016E+01	4.9345E+04 ± 4.0183E+01	2.2030E+03 ± 4.1941E+01
0.000320	-3.8205E+04 ± 9.0543E+00	4.0421E+04 ± 1.0403E+01	2.2164E+03 ± 1.3791E+01
0.001000	-3.0131E+04 ± 6.7318E+00	3.2404E+04 ± 2.0048E+01	2.2727E+03 ± 2.1148E+01
0.003200	-2.2592E+04 ± 4.6217E+00	2.4810E+04 ± 3.9682E+00	2.2180E+03 ± 6.0915E+00
0.010000	-1.5909E+04 ± 3.2149E+00	1.8126E+04 ± 7.9005E+00	2.2171E+03 ± 8.5296E+00

Relative difference using default slicing parameter: -2.0%
Factor of time the dipole implementation is faster: 3.7

Table 3: Numerical comparisons of our implementations of dipole subtraction and phase space slicing as described in Section 5, for $\sigma(p\bar{p} \to c\bar{c}[^3S_1^{[8]}] + X)$ (in nb) with $\sqrt{S} =$ 100 GeV, 2 GeV $< p_T <$ 3 GeV, and $-0.5 < y < 0.5$; $\sqrt{S} = 100$ GeV, 6 GeV $< p_T <$ 7 GeV, and $-0.5 < y < 0.5$; and $\sqrt{S} = 1.96$ TeV, 7 GeV $< p_T <$ 8 GeV, and $-0.6 < y < 0.6$. For a given value of δ (first column), the hard-collinear contribution of the real corrections (third column), the residual part including the soft and collinear contributions (second column), and their sum (forth column) are listed. The quoted errors are the numerical-integration uncertainties. For the default value $\delta = 10^{-3}$, the relative deviations of the phase space slicing results from the dipole subtraction ones and the factors by which the dipole subtraction implementation is faster than the space slicing one in achieving a numerical accuracy of 1% are indicated.

p+$\overline{\text{p}}$ --> c$\overline{\text{c}}$[3S18] + X: Sqrt[s] = 7000 GeV, 6 GeV < p_T < 8 GeV, 2.5 < y < 4:

Dipole implementation: 1.5209E+04 ± 1.5039E+01

Slicing implementation:

0.000010	-4.4765E+05 ± 1.3365E+02	4.5846E+05 ± 1.6483E+02	1.0810E+04 ± 2.1221E+02
0.000032	-3.7798E+05 ± 1.0265E+02	3.9071E+05 ± 7.0978E+01	1.2732E+04 ± 1.2480E+02
0.000100	-3.1423E+05 ± 8.1206E+01	3.2768E+05 ± 7.9244E+01	1.3452E+04 ± 1.1346E+02
0.000320	-2.5395E+05 ± 6.2502E+01	2.6789E+05 ± 3.1169E+01	1.3943E+04 ± 6.9842E+01
0.001000	-1.9945E+05 ± 4.4830E+01	2.1363E+05 ± 8.1179E+01	1.4182E+04 ± 9.2735E+01
0.003200	-1.4864E+05 ± 3.1923E+01	1.6281E+05 ± 1.6280E+01	1.4167E+04 ± 3.5834E+01
0.010000	-1.0368E+05 ± 2.1351E+01	1.1778E+05 ± 1.8833E+01	1.4097E+04 ± 2.8470E+01

Relative difference using default slicing parameter: -6.8%
Factor of time the dipole implementation is faster: 4.4

p+$\overline{\text{p}}$ --> c$\overline{\text{c}}$[3S18] + X: Sqrt[s] = 7000 GeV, 20 GeV < p_T < 22 GeV, -0.5 < y < 0.5:

Dipole implementation: 1.6314E+02 ± 1.8166E-01

Slicing implementation:

0.000010	-4.7483E+03 ± 1.4145E+00	4.8660E+03 ± 1.6862E+00	1.1770E+02 ± 2.2009E+00
0.000032	-4.0204E+03 ± 1.0596E+00	4.1628E+03 ± 1.0825E+00	1.4245E+02 ± 1.5148E+00
0.000100	-3.3545E+03 ± 8.1121E-01	3.5065E+03 ± 7.1555E-01	1.5199E+02 ± 1.0817E+00
0.000320	-2.7209E+03 ± 6.2684E-01	2.8762E+03 ± 4.7362E-01	1.5528E+02 ± 7.8565E-01
0.001000	-2.1458E+03 ± 4.6500E-01	2.3026E+03 ± 3.0469E-01	1.5681E+02 ± 5.5593E-01
0.003200	-1.6074E+03 ± 3.0795E-01	1.7633E+03 ± 1.9829E-01	1.5590E+02 ± 3.6627E-01
0.010000	-1.1275E+03 ± 2.1164E-01	1.2834E+03 ± 1.2832E-01	1.5587E+02 ± 2.4750E-01

Relative difference using default slicing parameter: -3.9%
Factor of time the dipole implementation is faster: 1.4

p+$\overline{\text{p}}$ --> c$\overline{\text{c}}$[3S18] + X: Sqrt[s] = 14000 GeV, 5 GeV < p_T < 8 GeV, 2 < y < 4:

Dipole implementation: 8.9783E+04 ± 8.9783E+01

Slicing implementation:

0.000010	-2.7420E+06 ± 8.3086E+02	2.8014E+06 ± 1.0012E+03	5.9400E+04 ± 1.3010E+03
0.000032	-2.3177E+06 ± 5.9967E+02	2.3901E+06 ± 7.6892E+02	7.2450E+04 ± 9.7511E+02
0.000100	-1.9297E+06 ± 4.9280E+02	2.0083E+06 ± 4.4693E+02	7.8650E+04 ± 6.6528E+02
0.000320	-1.5625E+06 ± 3.8080E+02	1.6439E+06 ± 2.9593E+02	8.1360E+04 ± 4.8227E+02
0.001000	-1.2304E+06 ± 2.8138E+02	1.3132E+06 ± 1.9530E+02	8.2850E+04 ± 3.4252E+02
0.003200	-9.2029E+05 ± 2.0434E+02	1.0037E+06 ± 1.2350E+02	8.3410E+04 ± 2.3876E+02
0.010000	-6.4571E+05 ± 1.3564E+02	7.2853E+05 ± 7.7187E+01	8.2820E+04 ± 1.5606E+02

Relative difference using default slicing parameter: -7.7%
Factor of time the dipole implementation is faster: 3.4

Table 4: Same as in Table 3, but for $\sqrt{S} = 7$ TeV, 6 GeV $< p_T <$ 8 GeV, and $2.5 < y < 4$; $\sqrt{S} = 7$ TeV, 20 GeV $< p_T <$ 22 GeV, and $-0.5 < y < 0.5$; and $\sqrt{S} = 14$ TeV, 5 GeV $< p_T <$ 8 GeV, and $2 < y < 4$.

```
p+p̄ --> cc̄[3P21] + X:  Sqrt[s] = 100 GeV,  2 GeV < p_T < 3 GeV,  -0.5 < y < 0.5:
================================================================================

Dipole implementation:   3.8434E+02 ± 3.8383E-01

Slicing implementation:
  0.000010    -1.9969E+04 ± 6.1018E+00     2.0204E+04 ± 8.2940E+00     2.3530E+02 ± 1.0297E+01
  0.000032    -1.6852E+04 ± 5.1391E+00     1.7156E+04 ± 5.5671E+00     3.0380E+02 ± 7.5765E+00
  0.000100    -1.4010E+04 ± 4.0109E+00     1.4355E+04 ± 3.6670E+00     3.4530E+02 ± 5.4345E+00
  0.000320    -1.1317E+04 ± 2.7969E+00     1.1679E+04 ± 2.3758E+00     3.6180E+02 ± 3.6697E+00
  0.001000    -8.8920E+03 ± 2.0774E+00     9.2572E+03 ± 1.5460E+00     3.6520E+02 ± 2.5895E+00
  0.003200    -6.6371E+03 ± 1.4326E+00     7.0012E+03 ± 9.6310E-01     3.6410E+02 ± 1.7262E+00
  0.010000    -4.6511E+03 ± 9.3505E-01     5.0079E+03 ± 5.8438E-01     3.5683E+02 ± 1.1026E+00

Relative difference using default slicing parameter: -5.0%
Factor of time the dipole implementation is faster: 137


p+p̄ --> cc̄[3P21] + X:  Sqrt[s] = 100 GeV,  6 GeV < p_T < 7 GeV,  -0.5 < y < 0.5:
================================================================================

Dipole implementation:  -1.1636E+00 ± 1.1635E-03

Slicing implementation:
  0.000010    -2.5001E+01 ± 4.9224E-03     2.3696E+01 ± 1.4019E-02    -1.3046E+00 ± 1.4858E-02
  0.000032    -2.1484E+01 ± 3.6945E-03     2.0258E+01 ± 9.5508E-03    -1.2264E+00 ± 1.0240E-02
  0.000100    -1.8219E+01 ± 3.1399E-03     1.7030E+01 ± 6.2299E-03    -1.1887E+00 ± 6.9764E-03
  0.000320    -1.5062E+01 ± 2.4189E-03     1.3884E+01 ± 4.1048E-03    -1.1778E+00 ± 4.7645E-03
  0.001000    -1.2145E+01 ± 1.8113E-03     1.0976E+01 ± 2.7625E-03    -1.1687E+00 ± 3.3033E-03
  0.003200    -9.3531E+00 ± 1.3760E-03     8.2043E+00 ± 1.6613E-03    -1.1488E+00 ± 2.1572E-03
  0.010000    -6.8082E+00 ± 9.9948E-04     5.7041E+00 ± 1.0307E-03    -1.1041E+00 ± 1.4357E-03

Relative difference using default slicing parameter: 0.4%
Factor of time the dipole implementation is faster: 4.3


p+p̄ --> cc̄[3P21] + X:  Sqrt[s] = 1960 GeV,  7 GeV < p_T < 8 GeV,  -0.6 < y < 0.6:
================================================================================

Dipole implementation:  -8.1975E+01 ± 1.0328E-01

Slicing implementation:
  0.000010    -2.4577E+03 ± 4.8300E-01     2.3627E+03 ± 1.5549E+00    -9.4960E+01 ± 1.6282E+00
  0.000032    -2.1184E+03 ± 3.8233E-01     2.0317E+03 ± 1.0440E+00    -8.6660E+01 ± 1.1118E+00
  0.000100    -1.8032E+03 ± 3.1323E-01     1.7206E+03 ± 7.0188E-01    -8.2550E+01 ± 7.6860E-01
  0.000320    -1.4983E+03 ± 2.3867E-01     1.4167E+03 ± 4.6731E-01    -8.1640E+01 ± 5.2473E-01
  0.001000    -1.2168E+03 ± 1.9288E-01     1.1358E+03 ± 3.2025E-01    -8.1050E+01 ± 3.7385E-01
  0.003200    -9.4671E+02 ± 1.4560E-01     8.6743E+02 ± 2.1682E-01    -7.9280E+01 ± 2.6117E-01
  0.010000    -6.9965E+02 ± 1.0889E-01     6.2487E+02 ± 1.4362E-01    -7.4780E+01 ± 1.8023E-01

Relative difference using default slicing parameter: -1.1%
Factor of time the dipole implementation is faster: 2.3
```

Table 5: Same as in Table 3, but for $\sigma(p\bar{p} \to c\bar{c}[^3P_2^{[1]}] + X)$.

p+$\overline{\text{p}}$ --> c$\overline{\text{c}}$[3P21] + X: Sqrt[s] = 7000 GeV, 6 GeV < p_T < 8 GeV, 2.5 < y < 4:

Dipole implementation: -5.0338E+02 ± 8.1114E-01

Slicing implementation:

0.000010	-2.1012E+04 ± 4.3885E+00	2.0323E+04 ± 1.4953E+01	-6.8870E+02 ± 1.5584E+01
0.000032	-1.8013E+04 ± 3.3649E+00	1.7425E+04 ± 9.6143E+00	-5.8830E+02 ± 1.0186E+01
0.000100	-1.5239E+04 ± 2.8673E+00	1.4677E+04 ± 6.5227E+00	-5.6230E+02 ± 7.1251E+00
0.000320	-1.2574E+04 ± 2.2069E+00	1.2041E+04 ± 4.2413E+00	-5.3310E+02 ± 4.7811E+00
0.001000	-1.0127E+04 ± 1.6732E+00	9.6082E+03 ± 2.8694E+00	-5.1900E+02 ± 3.3216E+00
0.003200	-7.7997E+03 ± 1.2484E+00	7.2897E+03 ± 1.9169E+00	-5.1000E+02 ± 2.2876E+00
0.010000	-5.6897E+03 ± 8.9294E-01	5.2073E+03 ± 1.2364E+00	-4.8240E+02 ± 1.5251E+00

Relative difference using default slicing parameter: 3.1%
Factor of time the dipole implementation is faster: 2.1

p+$\overline{\text{p}}$ --> c$\overline{\text{c}}$[3P21] + X: Sqrt[s] = 7000 GeV, 20 GeV < p_T < 22 GeV, -0.5 < y < 0.5:

Dipole implementation: -1.0014E+01 ± 1.0013E-02

Slicing implementation:

0.000010	-6.9249E+01 ± 1.5399E-02	5.8884E+01 ± 2.9578E-02	-1.0365E+01 ± 3.3346E-02
0.000032	-6.1220E+01 ± 1.3769E-02	5.1169E+01 ± 1.4606E-02	-1.0051E+01 ± 2.0073E-02
0.000100	-5.3471E+01 ± 1.2195E-02	4.3475E+01 ± 9.2384E-03	-9.9958E+00 ± 1.5299E-02
0.000320	-4.5673E+01 ± 1.0564E-02	3.5722E+01 ± 6.4647E-03	-9.9510E+00 ± 1.2385E-02
0.001000	-3.8146E+01 ± 8.9563E-03	2.8256E+01 ± 4.7210E-03	-9.8900E+00 ± 1.0124E-02
0.003200	-3.0578E+01 ± 7.2845E-03	2.0851E+01 ± 3.4411E-03	-9.7273E+00 ± 8.0564E-03
0.010000	-2.3281E+01 ± 5.6306E-03	1.3958E+01 ± 2.3551E-03	-9.3230E+00 ± 6.1032E-03

Relative difference using default slicing parameter: -1.2%
Factor of time the dipole implementation is faster: 0.48

p+$\overline{\text{p}}$ --> c$\overline{\text{c}}$[3P21] + X: Sqrt[s] = 14000 GeV, 5 GeV < p_T < 8 GeV, 2 < y < 4:

Dipole implementation: -1.5363E+03 ± 5.4212E+00

Slicing implementation:

0.000010	-1.6753E+05 ± 4.0603E+01	1.6446E+05 ± 4.5001E+01	-3.0702E+03 ± 6.0611E+01
0.000032	-1.4322E+05 ± 3.0717E+01	1.4094E+05 ± 3.8639E+01	-2.2820E+03 ± 4.9361E+01
0.000100	-1.2083E+05 ± 2.4876E+01	1.1889E+05 ± 2.0610E+01	-1.9426E+03 ± 3.2305E+01
0.000320	-9.9425E+04 ± 2.0367E+01	9.7638E+04 ± 1.3883E+01	-1.7870E+03 ± 2.4648E+01
0.001000	-7.9823E+04 ± 1.4390E+01	7.8121E+04 ± 9.4865E+00	-1.7020E+03 ± 1.7235E+01
0.003200	-6.1268E+04 ± 1.0435E+01	5.9614E+04 ± 6.3932E+00	-1.6540E+03 ± 1.2238E+01
0.010000	-4.4537E+04 ± 7.2279E+00	4.2986E+04 ± 4.3827E+00	-1.5510E+03 ± 8.4528E+00

Relative difference using default slicing parameter: 10.8%
Factor of time the dipole implementation is faster: 3.3

Table 6: Same as in Table 4, but for $\sigma(p\bar{p} \to c\bar{c}[^3P_2^{[1]}] + X)$.

and Research BMBF through Grant No. 05H15GUCC1 and by the German Research Foundation DFG through Grant No. KN 365/12-1.

References

[1] G. T. Bodwin, E. Braaten, and G. P. Lepage, Rigorous QCD analysis of inclusive annihilation and production of heavy quarkonium, Phys. Rev. D **51**, 1125 (1995); **55**, 5853(E) (1997) [arXiv:hep-ph/9407339].

[2] W. E. Caswell and G. P. Lepage, Effective Lagrangians For Bound State Problems In QED, QCD, And Other Field Theories, Phys. Lett. B **167**, 437 (1986).

[3] G. P. Lepage, L. Magnea, C. Nakhleh, U. Magnea, and K. Hornbostel, Improved nonrelativistic QCD for heavy quark physics, Phys. Rev. D **46**, 4052 (1992) [hep-lat/9205007].

[4] B. W. Harris and J. F. Owens, The Two cutoff phase space slicing method, Phys. Rev. D **65**, 094032 (2002) [hep-ph/0102128].

[5] J. M. Campbell, F. Maltoni, and F. Tramontano, QCD corrections to J/psi and Upsilon production at hadron colliders, Phys. Rev. Lett. **98**, 252002 (2007) [hep-ph/0703113]; P. Artoisenet, J. M. Campbell, J. P. Lansberg, F. Maltoni, and F. Tramontano, Υ Production at Fermilab Tevatron and LHC Energies, Phys. Rev. Lett. **101**, 152001 (2008) [arXiv:0806.3282 [hep-ph]]; P. Artoisenet, J. M. Campbell, F. Maltoni, and F. Tramontano, J/psi production at HERA, Phys. Rev. Lett. **102**, 142001 (2009) [arXiv:0901.4352 [hep-ph]].

[6] S. Catani and M. H. Seymour, A General algorithm for calculating jet cross-sections in NLO QCD, Nucl. Phys. **B485**, 291 (1997); **B510**, 503(E) (1998) [hep-ph/9605323].

[7] M. Butenschoen and B. A. Kniehl, Dipole subtraction at next-to-leading order in nonrelativistic-QCD factorization, Nucl. Phys. **B950**, 114843 (2020) [arXiv:1909.03698 [hep-ph]].

[8] L. Phaf and S. Weinzierl, Dipole formalism with heavy fermions, J. High Energy Phys. 04 (2001) 006 [hep-ph/0102207].

[9] F. V. Tkachov, A Theorem on Analytical Calculability of Four Loop Renormalization Group Functions, Phys. Lett. **100B**, 65 (1981); K. G. Chetyrkin and F. V. Tkachov, Integration by Parts: The Algorithm to Calculate beta Functions in 4 Loops, Nucl. Phys. B **192**, 159 (1981).

[10] M. Butenschön and B. A. Kniehl, Complete next-to-leading-order corrections to J/ψ photoproduction in nonrelativistic quantum chromodynamics, Phys. Rev. Lett. **104**, 072001 (2010) [arXiv:0909.2798 [hep-ph]]; Reconciling J/ψ production at HERA,

RHIC, Tevatron, and LHC with NRQCD factorization at next-to-leading order, Phys. Rev. Lett. **106**, 022003 (2011) [arXiv:1009.5662 [hep-ph]]; World data of J/ψ production consolidate NRQCD factorization at NLO, Phys. Rev. D **84**, 051501(R) (2011) [arXiv:1105.0820 [hep-ph]]; Probing nonrelativistic QCD factorization in polarized J/ψ photoproduction at next-to-leading order, Phys. Rev. Lett. **107**, 232001 (2011) [arXiv:1109.1476 [hep-ph]]; Next-to-leading-order tests of NRQCD factorization with J/ψ yield and polarization, Mod. Phys. Lett. A **28**, 1350027 (2013) [arXiv:1212.2037 [hep-ph]]; M. Butenschoen, Z.-G. He, and B. A. Kniehl, NLO NRQCD disfavors the interpretation of X(3872) as $\chi_{c1}(2P)$, Phys. Rev. D **88**, 011501(R) (2013) [arXiv:1303.6524 [hep-ph]]; η_c production at the LHC challenges nonrelativistic-QCD factorization, Phys. Rev. Lett. **114**, 092004 (2015) [arXiv:1411.5287 [hep-ph]].

[11] M. Butenschoen and B. A. Kniehl, J/ψ polarization at Tevatron and LHC: Nonrelativistic-QCD factorization at the crossroads, Phys. Rev. Lett. **108**, 172002 (2012) [arXiv:1201.1872 [hep-ph]].

[12] M. Butenschoen, Z.-G. He, and B. A. Kniehl, Deciphering the $X(3872)$ via its polarization in prompt production at the CERN LHC, Phys. Rev. Lett. **123**, 032001 (2019) [arXiv:1906.08553 [hep-ph]].

[13] H.-F. Zhang, L. Yu, S.-X. Zhang, and L. Jia, Global analysis of the experimental data on χ_c meson hadroproduction, Phys. Rev. D **93**, 054033 (2016); **93**, 079901(E) (2016) [arXiv:1410.4032 [hep-ph]].

[14] B. Gong, L.-P. Wan, J.-X. Wang, and H.-F. Zhang, Polarization for Prompt J/ψ and $\psi(2s)$ Production at the Tevatron and LHC, Phys. Rev. Lett. **110**, 042002 (2013) [arXiv:1205.6682 [hep-ph]].

[15] Y. Feng, B. Gong, C.-H. Chang, and J.-X. Wang, Remaining parts of the long-standing J/ψ polarization puzzle, Phys. Rev. D **99**, 014044 (2019) [arXiv:1810.08989 [hep-ph]].

[16] J. Pumplin, D. R. Stump, J. Huston, H.-L. Lai, P. Nadolsky, and W.-K. Tung, New generation of parton distributions with uncertainties from global QCD analysis, J. High Energy Phys. 07 (2002) 012 [hep-ph/0201195].